

# Frequency-Sweep Examination for Wave Mode Identification in Multimodal Ultrasonic Guided Wave Signal

Sina Fateri, *Student Member, IEEE*, Nikolaos V. Boulgouris, *Senior Member, IEEE*, Adam Wilkinson, Wamadeva Balachandran, *Fellow, IEEE*, and Tat-Hean Gan

**Abstract**—Ultrasonic guided waves can be used to assess and monitor long elements of a structure from a single position. The greatest challenges for any guided wave system are the plethora of wave modes arising from the geometry of the structural element which propagate with a range of frequency-dependent velocities and the interpretation of these combined signals reflected by discontinuities in the structural element. In this paper, a novel signal processing technique is presented using a combination of frequency-sweep measurement, sampling rate conversion, and Fourier transform. The technique is applied to synthesized and experimental data to identify different modes in complex ultrasonic guided wave signals. It is demonstrated throughout the paper that the technique also has the capability to derive the time of flight and group velocity dispersion curve of different wave modes in field inspections.

## I. INTRODUCTION

ULTRASONIC guided waves (UGWs) have been used in the last few years to examine the health of structural components of varied geometries; principally for detection of flaws, corrosion, and metal loss. In the case of one-dimensional structures, e.g., pipes, the reflected guided waves are measured and translated into defect categorization, giving parameters including total cross sectional area and through-wall depth of the defect [1]. Although many recent techniques are evolving into promising inspection tools, several challenges still exist. UGWs give rise to multiple wave modes within a frequency region with a dispersive nature because their velocities can be frequency dependent. In addition, signal interpretations are often difficult because of multimode propagation and mode conversion, along with test structure geometric features [2]. These limitations influence design procedures and software preconditioning, which consequently affects the overall performance of UGW inspections.

Dispersion curves deliver useful quantitative information in any UGW inspection system. A dispersion curve diagram illustrates the frequency or wavenumber relation

to the wave velocity in separate curves for existing modes in a frequency region. These are curves of the variation in phase and group velocity ( $v_{ph}$  and  $v_{gr}$ ) over a range of frequencies for each wave mode. The gradient of the phase velocity dispersion curve for a nondispersive wave mode over a particular frequency range, will be flat over that bandwidth; therefore, phase velocity will be quite close to group velocity [3]. On the other hand, dispersive signals have a tendency to spread out over time and space as the phase will be traveling with a different velocity ( $v_{ph}$ ) to the envelope ( $v_{gr}$ ). Thus, multimode dispersive propagation is a more challenging scenario for UGW inspections. Fig. 1 represents the group velocity dispersion curves for an 8-mm-diameter aluminum rod plotted by the Disperse software designed and developed by Imperial College London [4]. As can be seen in Fig. 1, numerous dispersive and nondispersive wave modes exist across the frequency regions which superpose to confuse the inspection. An effective technique is therefore required to identify the constituent elements for a reliable interpretation.

Alleyne and Cawley [5] demonstrated how two-dimensional data are required to achieve wave mode isolation, using time-domain data collected from several equally spaced points on the surface of a pipe along the axis. This is a useful method from a research point of view, but inconvenient for field inspections in a pitch-catch experiment. This requires either an array of transducers or laser vibrometry equipment, which can be expensive and/or time consuming. Prosser and Seale [6] used a time-frequency analysis (the pseudo-Wigner-Ville distribution) and managed to characterize the Lamb-mode dispersion and recover a part of the dispersion curve of the wave modes. Wilcox *et al.* [7] presented a technique for modeling the propagation of a dispersive wave packet. They also introduced a minimum resolvable distance (MRD) which could facilitate the minimization of the wave packet's duration after a given propagation distance.

Sicard *et al.* [8] and Wilcox [9] presented a method to compensate the effect of dispersion from UGW signal. However, the method only works for a specified wave mode, in a particular structure, with known dispersion characteristics within the signal bandwidth. Later, Toyama and Hayashi [10] proposed a dispersion compensation method using pulse compression to remove the effect of velocity dispersion and improve the SNR. Kuttig *et al.* [11], used the time-frequency representation (TFR) spectrogram and chirplet transform to extract the propor-

Manuscript received March 3, 2014; accepted June 2, 2014. The work is financially sponsored by the Engineering and Physical Sciences Research Council (EPSRC), TWI Ltd., and the Centre for Electronic Systems Research (CESR) of Brunel University, London, UK.

S. Fateri, N. V. Boulgouris, and W. Balachandran are with Center for Electronic Systems Research (CESR), Brunel University, London, UK (e-mail: Sina.Fateri@brunel.ac.uk).

S. Fateri, A. Wilkinson, and T.-H. Gan are with TWI Ltd. Granta Park, Cambridge, Cambridgeshire, UK.

DOI <http://dx.doi.org/10.1109/TUFFC.2014.3065>

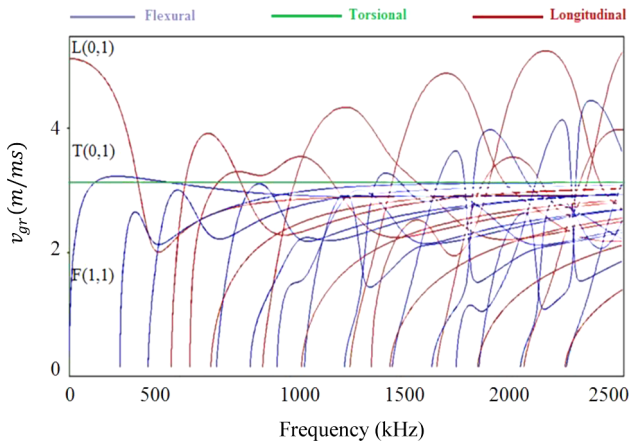



Fig. 1. Group velocity dispersion curve of an aluminum rod. 

tional energy distribution of a single wave mode from a multimode dispersive signal. Minozio *et al.* [12], proposed a technique using singular value decomposition (SVD) and managed to recover a UGW phase velocity dispersion curve. However, the technique requires measurements of several propagation distances. Xu *et al.* [13] used a crazy-climber algorithm to separate time-frequency ridges of individual modes from TFR ridges. However, there were some limitations because of the difficulty in identification of some modes. Moreover, the application of this technique is restricted by the requirement for manual intervention. Song *et al.* [14] used a blind identification algorithm via the joint approximate diagonalization of eigenmatrices (JADE). They suggested that the JADE algorithm may be used to separate the superposed signals and could potentially be used to evaluate long bones. However, such an approach requires multi-measured acquisitions concurrently. Recently, Xu *et al.* successfully solved the single-mode limitation of the traditional dispersion compensation methods and further proposed a multimode compensation technique [15] with the advantages of selective mode separation and parameter estimation. However, because all of the dispersion compensation methods make use of *a priori* knowledge of the dispersion curve, further improvements are still required. Thus, according to the literature, an effective and automatic technique to identify UGW modes remains a challenge in signal processing for UGW inspections.

## II. PROPOSED TECHNIQUE

In this paper, a novel signal processing technique is developed using the combination of sampling rate conversion in fractional-ratio, Fourier transform, and the concept of frequency sweep spectrum (FSS) to identify different wave modes in a complex UGW response including several superposed signals. Specifically, accurate quantitative information, such as total number of existing wave modes in a particular frequency range, number of constituent wave packets in a superposed signal, and  $v_{gr}$  of a wave mode

by extracting the time-of-flight (ToF), is to be taken out from the technique outcome to ease the defect detection process. The technique employs multiple-cycle Hann-windowed sinusoidal pulse train [16], [17] excitations at a range of UGW frequencies which are equally incremented. It proposes to identify signals with similar group velocities but different gradient arising from independent modes.

It is shown that the rate-converted time shift caused by sampling rate conversion for each signal can adjust their operating frequency to the frequency of interest. Consequently, this promotes sequential rate-converted time shifts to the individual acquisitions at each frequency increment. Hence, the technique can exploit the different gradients of the lines corresponding to each wave mode in the group velocity dispersion curve, which facilitates the identification of different wave modes in the superposed signals. It is also best suited for one-dimensional structures e.g., rods, bars, pipes, rails, etc.

The methodology is initially applied to synthesized data performed by Matlab-R2011b and then validated using experimental data collected using a Teletest Focus pulser/receiver (TWI Ltd., Cambridge, UK).

### A. Data Collection

To extract useful information from the application of the frequency-sweep examination (FSE) technique, the data collection must follow a particular routine. The UGW excitations should cover a wide range of UGW frequencies starting from  $f_0$  to  $f_{p-1}$  with equal incremental factor ( $q$ ). The acquisitions  $x_\alpha(t)$ , with the excitation index of  $\alpha = \{0, 1, 2, \dots, p-1\}$  are arranged in a matrix with  $p$  different steps/rows at each excitation frequency. Therefore, the frequency-sweep increment ( $q$ ) and the acquisition matrix can be expressed, respectively, as

$$q = \frac{f_{p-1} - f_0}{(p-1)}, \quad \forall p \in \mathbb{N} \quad (1)$$

$$I_{p \times c}(t, f) = \begin{bmatrix} x_1(t) \\ x_2(t) \\ \vdots \\ x_p(t) \end{bmatrix}_{p \times c} = \begin{bmatrix} I_{11} & \dots & I_{1c} \\ \vdots & \ddots & \vdots \\ I_{(p-1)1} & \dots & I_{(p-1)c} \\ I_{p1} & \dots & I_{pc} \end{bmatrix}, \quad (2)$$

where  $c$  is the number of columns in the matrix, which represents the length of each single acquisition,  $f_{p-1}$  is the upper limit of frequency-sweep, and  $f_0$  is the lower limit.

A constant appropriate sampling rate [18] is used for each acquisition in the array,  $x_\alpha(t)$ , which satisfies the Nyquist criterion for the highest frequency/bandwidth acquisition. The criteria for the choice of  $p$  and  $q$  is discussed in later sections in the context of data accuracy.

### B. Sampling Rate Conversion

Each acquisition  $x(t)$  is transformed to a new signal  $y(\tau)$  as defined in (2) and (7) by fractional ratio sampling

rate conversion [19]. For each signal, a spline [20] is fitted to the samples to reconstruct the original signals. Sampling starts at the beginning of the signal so that the first sample is common to both  $x(t)$  and  $y(\tau)$ . The fractional ratio for each transformation is chosen and defined in (3) and (4) according to the frequency of excitation, so that each signal appears to have the same excitation frequency as  $f_0$ . Thus, the acquisitions will be ready for the direct comparison along the rate-converted frequency-sweep axis.

Series of fractional sampling rate conversions are applied to each acquisition to rate convert over the entire range of frequencies, ( $f_0$  to  $f_{p-1}$ ) and adjust them back to the  $f_0$  frequency. Therefore, it can facilitate the extraction of quantitative information; i.e., ToF and group velocity at  $f_0$  after the application of the Fourier transform. The fractional-ratio converter can be made by arranging two integer-ratio converters  $M$  and  $L$  in series. The input sampling rate is multiplied by  $L$  in an interpolator, and the result is divided by  $M$  in a downsampler. Therefore, the general fractional ratio can be expressed as

$$\frac{T'_s}{T_s} = \frac{M}{L} = R \quad \text{or} \quad F'_s = \frac{L}{M} F_s = F_s/R, \quad (3)$$

where  $T_s$ ,  $T'_s$  and  $F_s$ ,  $F'_s$  are the input and output sampling intervals and sampling frequencies, respectively.

In this paper, we consider an adaptive ratio ( $R_\alpha$ ) for each frequency-sweep excitation:

$$R_\alpha = M/L = \omega_\alpha/\omega_0, \quad (4)$$

where  $\omega_0$  and  $\omega_\alpha$  are the angular velocity at  $f_0$  and successive sweeping frequencies,  $f_\alpha$ , respectively, defined as

$$\omega_0 = 2\pi f_0, \quad \omega_\alpha = 2\pi f_\alpha. \quad (5)$$

Thus, the output of the sampling rate conversion,  $y(\tau)$  can be expressed in terms of interpolation and downsampling as [21],

$$y_\alpha(\tau) = \sum_{t=-\infty}^{\infty} h(tL + \tau M \oplus L)x(\tau R_\alpha - t), \quad (6)$$

where  $h(k)$  is a digital filter which operates both downsampling and interpolation process.

Thus, according to the input matrix given in (2) and the aforementioned sampling rate conversion, the output of the rate-converted set of acquisitions can be expressed as

$$\tilde{O}_{p \times z}(\tau, \alpha) = \begin{bmatrix} y_1(\tau) \\ y_2(\tau) \\ \vdots \\ y_p(\tau) \end{bmatrix}_{p \times z} = \begin{bmatrix} o_{11} & \cdots & o_{1z} \\ \vdots & \ddots & \vdots \\ o_{(p-1)1} & \cdots & o_{(p-1)z} \\ o_{p1} & \cdots & o_{pz} \end{bmatrix}, \quad (7)$$

where  $\tau$  is the rate-converted time and  $z$  is the number of columns in the matrix, which represents the length of each rate-converted acquisition given after the sampling rate conversion. It is also notable that the number of columns changed (from  $c$  to  $z$ ) because of the effect of sampling rate conversion on the length of each acquisition. This change in the length creates the rate-converted time ( $\tau$ ), which is constructed based on the sample shifts caused after the sampling rate conversion. For each individual acquisition, zero-paddings may be needed to create the  $\tilde{O}_{p \times z}$  matrix, because they are rate-converted with different fractional ratios defined in (4).

After the sampling rate conversion, all of the acquisitions appear as if excited at the same frequency as  $f_0$ . Therefore, the excitation index ( $\alpha$ ) has been set as the variable of the column vectors. Here, the amplitude sweep wave form (ASW) can be defined as

$$ASW_1(\alpha) = \begin{Bmatrix} o_{11} \\ \vdots \\ o_{(p-1)1} \\ o_{p1} \end{Bmatrix}, \dots, ASW_z(\alpha) = \begin{Bmatrix} o_{1z} \\ \vdots \\ o_{(p-1)z} \\ o_{pz} \end{Bmatrix}. \quad (8)$$

It is constructed as the combination of single value amplitude information of the sampling rate-converted acquisitions for a point in rate-converted time defined in (7). Sample ASWs are illustrated in Sections III and IV. It is notable that the  $x$ -axis represents the samples collected from the individual rate-converted frequency-sweep acquisitions. They show how several superposed signals can be represented in different oscillations.

### C. Fourier Transform of the Signal Array

To obtain the spectrum of the incremental variations after the sampling rate conversion, the ASWs defined in (8) should be Fourier transformed. This will reveal the spectrum of incremental variations for each fixed point in rate-converted time which is called frequency sweep spectrum (FSS). The FSS measures the rate of shifts in rate-converted time for various wave modes in number of cycles per sample.

According to the time-domain system input-output given in (2) and (7), the transform relationships of the individual integer downsampling and interpolation system, the output spectrum  $FSS(f)$  can be determined in terms of the input  $ASW(\alpha)$  as

$$FSS(\tilde{f}) = \sum_{\alpha=0}^{p-1} ASW(\alpha) \cdot e^{-j2\pi\tilde{f}\alpha}. \quad (9)$$

Thus, the total frequency-sweep spectrum (TFSS) of the signal array can be expressed as

$$\begin{aligned} \text{TFSS}_{z \times w}(\tilde{f}, \tau) &= \begin{bmatrix} \sum_{\alpha=0}^{p-1} ASW_1(\alpha) \cdot e^{-j2\pi\tilde{f}\alpha} \\ \vdots \\ \sum_{\alpha=0}^{p-1} ASW_{z-1}(\alpha) \cdot e^{-j2\pi\tilde{f}\alpha} \\ \sum_{\alpha=0}^{p-1} ASW_z(\alpha) \cdot e^{-j2\pi\tilde{f}\alpha} \end{bmatrix} \\ &= \begin{bmatrix} f_{11} & \cdots & f_{1w} \\ \vdots & \ddots & \vdots \\ f_{(z-1)1} & \cdots & f_{(z-1)z} \\ f_{z1} & \cdots & f_{zw} \end{bmatrix}. \end{aligned} \quad (10)$$

The incremental variations correspond to individual rows in the TFSS<sub>z×w</sub> matrix, which include individual FSS( $\tilde{f}$ ) at each instant in rate-converted time. This facilitates the identification of existing wave modes at  $f_0$  in Fourier domain and extraction of the ToF using a threshold based on the specific value sensitive to the level of coherent noise [22] according to the measured SNR at  $f_0$ .

#### D. Data Accuracy

As discussed in Section II-A, a constant appropriate sampling rate was used for each acquisition in the array which could satisfy the Nyquist criterion for the highest frequency/bandwidth acquisition. However, the accuracy of the ASWs depends on choosing an appropriate number of frequency-sweep acquisitions,  $p$ . Fig. 2 shows the echoes from a nondispersive wave modes [e.g., the L(0,1) wave mode in the rod under investigation] which have a linearly increasing shift in rate-converted time as the frequency of excitation increases from  $f_0$  to  $f_{p-1}$ . Fig. 2 also shows a pictorial representation of the variables used in subsequent equations.

The maximum rate-converted time shift caused by sampling rate conversion for a nondispersive signal can be expressed as

$$t'_{\text{FSE}} = (t_{\text{FSE}}) \left( \frac{f_{p-1}}{f_0} \right), \quad (11)$$

where  $t_{\text{FSE}}$  is the lowest experienced rate-converted time shift caused by the sampling rate conversion.

The shift between  $f_0$  and adjacent vertical sample can be expressed as

$$\Delta t_{\text{FSE}} = t'_{\text{FSE}} - t_{\text{FSE}} = \left( \frac{f_{p-1}}{f_0} - 1 \right) \left( \frac{t_{\text{FSE}}}{p} \right). \quad (12)$$

It is known [23] that the frequency band  $B$  of an  $n$ -cycle Hann windowed sine wave at  $f_0$  which corresponds to the excitation signal is expressed as

$$B = [f_0 - 2f_0/n : f_0 + 2f_0/n]. \quad (13)$$

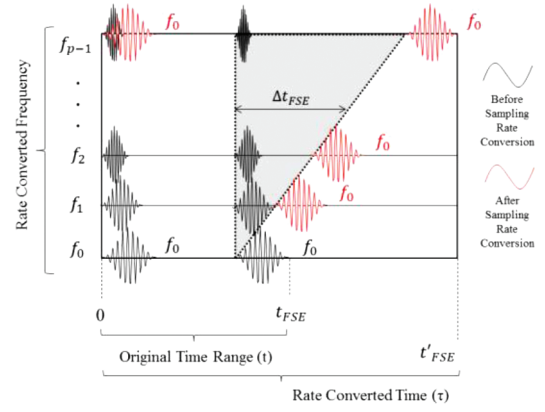


Fig. 2. Theoretical signals before ( $I_{p \times c}$ ) and after ( $\tilde{O}_{p \times z}$ ) sampling rate conversion.

Thus, according to (11), (12), and the Nyquist criterion, the minimum number of steps ( $p$ ) should comply with

$$\frac{p}{((f_{p-1}/f_0) - 1)(t_{\text{FSE}})} > (f_0 + 2f_0/n). \quad (14)$$

As a result, the necessary range for  $p$  is

$$p > (f_0 + 2f_0/n)((f_{p-1}/f_0) - 1)(t_{\text{FSE}}). \quad (15)$$

It is sufficient for the necessary range for  $p$  to be rounded to the next power of two, so as to perform a computationally efficient Fourier analysis.

In addition, according to the dispersion curve shown in Fig. 1, the velocity and the ToF of a wave mode may tend to vary and/or remain constant in a certain frequency region depending on its dispersive and/or nondispersive propagation. Subsequently, these variations change the gradient of the rate-converted time shift after sampling rate conversion. Therefore, an alternative way to increase the data resolution in the system output, or change the gradient of the rate-converted time shift, is to shorten the original time range to detect the presence of different wave modes.

#### E. Group Velocity Value Extraction

According to information given in Section II-C, and assuming that the length of propagation is known ( $l$ ), the group velocity value at  $f_0$  can be extracted by

$$v_{\text{gr}} = \frac{l}{t_{\text{ToF}}}, \quad (16)$$

where  $t_{\text{ToF}}$  is the extracted ToF of the wave mode of interest.

The group velocity dispersion curve can also be computed by frequently applying the FSE procedure to the input matrix given in (2) with a given gradual change in the value of the  $f_0$  frequency, so that the group velocity at that frequency could be extracted sequentially.



### F. FSE Summary and Analysis

For each of the frequency-sweep experiments, the time duration of the  $n$ -cycle excitation pulse is reduced. As a consequence, the time duration of the reflected signals (especially the nondispersive signals) is also reduced.

For nondispersive signals in the frequency-sweep acquisitions, the increasing shift associated with the sampling rate conversion is linearly related to the increasing excitation frequency. Therefore, they can possess a constant frequency in the FSS domain. Fig. 2 shows this effect for the nondispersive signals. For dispersive signals, the variations of group and phase velocity with respect to excitation frequency will cause a shift in the time domain even before sampling rate conversion. However, these shifts cannot be traced with ASWs/FSSs because of the presence of different excitation frequencies in each acquisition. After sampling rate conversion, the acquisitions appear as if they were excited at the same frequency as  $f_0$ . Therefore, a more exaggerated nonlinear shift can be experienced by dispersive signals, which can potentially exhibit higher frequency in  $\text{FSS}(\tilde{f})$  compared with the nondispersive signals. These different frequencies in  $\text{FSS}(\tilde{f})$  facilitate the identification of different dispersive and nondispersive signals. As a result, the superposed signals should possess different oscillations in the  $\text{ASW}(\alpha)$  and appear as clear peaks in the  $\text{FSS}(\tilde{f})$ , which facilitates the extraction of ToF and group velocity of the constituent wave modes.

To summarize, the steps in applying the FSE are as follows:

- Collect the frequency-sweep acquisitions,  $x_a(t)$  based on (1), (2), and (15), from  $f_0$  to  $f_{p-1}$ .
- Apply the sampling rate conversion with the ratios given in (4). Therefore, all of the acquisitions should appear as if excited at the same frequency as  $f_0$ .
- Construct the  $\text{ASW}(\alpha)$  based on (7) and (8).
- Perform the Fourier transform on the  $\text{ASW}(\alpha)$  at the entire rate-converted time range to obtain the  $\text{FSS}(\tilde{f})$  based on (9).
- Collect the whole obtained  $\text{FSS}(\tilde{f})$  to produce  $\text{TFSS}(\tilde{f}, \tau)$  based on (10).
- While performing the Fourier transform and constructing the  $\text{TFSS}(\tilde{f}, \tau)$ , define a threshold value sensitive to the level of coherent noise (according to the already measured SNR at  $f_0$ ) to automatically identify the existence of the wave modes in a superposed wave packet.
- Perform peak searches in the responses given by  $\text{FSS}(\tilde{f})$  to extract the number of existing wave modes in a superposed wave packet with their ToF information.
- Compute the group velocity at  $f_0$  based on (16).
- Repeat the whole process from the start with a given gradual change in  $f_0$  to compute the desired portion of group velocity dispersion curve.

### III. SIGNAL SYNTHESIS

Signals were synthesized to examine the FSE proposed in Section II. The technique is applied to superposed complex wave packets representing the interaction between  $L(0,1)$  and  $F(1,1)$  [24] propagating wave modes. A dispersion simulation was carried out as a part of the synthesis.

#### A. Wave Modes Analysis

A superposed wave packet comprising  $L(0,1)$  and  $F(1,1)$  wave modes were synthesized based on the group velocity dispersion curve given in Fig. 1 to identify them with the aid of FSE procedure. Fig. 3(left) illustrates sample isolated and superposed wave modes as a result of 20-kHz, 10-cycle Hann windowed excitation. With reference to Section II-A and Section II-D, a set of 512 superposed signals were generated from  $f_0$  (20 kHz) to  $f_{p-1}$  (100 kHz) and were rate-converted back to  $f_0$  20 kHz.

The simulation of dispersive  $F(1,1)$  wave mode was performed according to the method described by Wilcox *et al.* [7] using the parameters given in the dispersion curve. In this case, it was assumed that the transducer is ideal and only excites the guided wave modes of interest at the given location.

Three sample  $\text{FSS}(\tilde{f})$ s of the isolated  $L(0,1)$ ,  $F(1,1)$  and their superposition at 2300  $\mu\text{s}$  are displayed in Fig. 3(middle).

Fig. 3(right) illustrates contour plots of the  $\text{TFSS}(\tilde{f}, \tau)$  measured at the entire rate-converted time instants. The distinct curves illustrated in Fig. 3(right) are traced energy peaks which show the discriminated wave modes of interest and the ability of FSE to identify the superposed wave modes at the frequency of interest where signals are overlapped, i.e.,  $f_0$ , 20 kHz.

According to the discussion provided in Section II, each row of the rate-converted output matrix given in (7) contains superposed signals where each is gradually shifted in rate-converted time. The spectrum of the acquisition signals before the sampling rate conversion, gives no indication as to how the frequency content of a signal changes with the  $\text{FSS}(\tilde{f})$  of the signal at each single rate-converted time instant. However; after sampling rate conversion, all of the nondispersive and dispersive signals of the frequency-sweep acquisition appear as if excited at the same frequency as  $f_0$ , while experiencing different shifts in rate-converted time as the excitation frequency increases, because of the existence of flat and nonlinear group velocity dispersion curves, respectively. These different shifts in rate-converted time (linear/nonlinear) after sampling rate conversion, facilitate a situation in which each column of the  $\tilde{O}_{p \times z}(\tau, f)$  matrix to be selected as  $\text{ASW}(\alpha)$  has different oscillations e.g., Fig. 4. These different oscillations in the selected ASWs defined in (8) contain key information about any nondispersive and dispersive signals which classify each single reflection in different oscillations. It is notable that the  $x$ -axis of the  $\text{ASW}(\alpha)$  represents the indi-

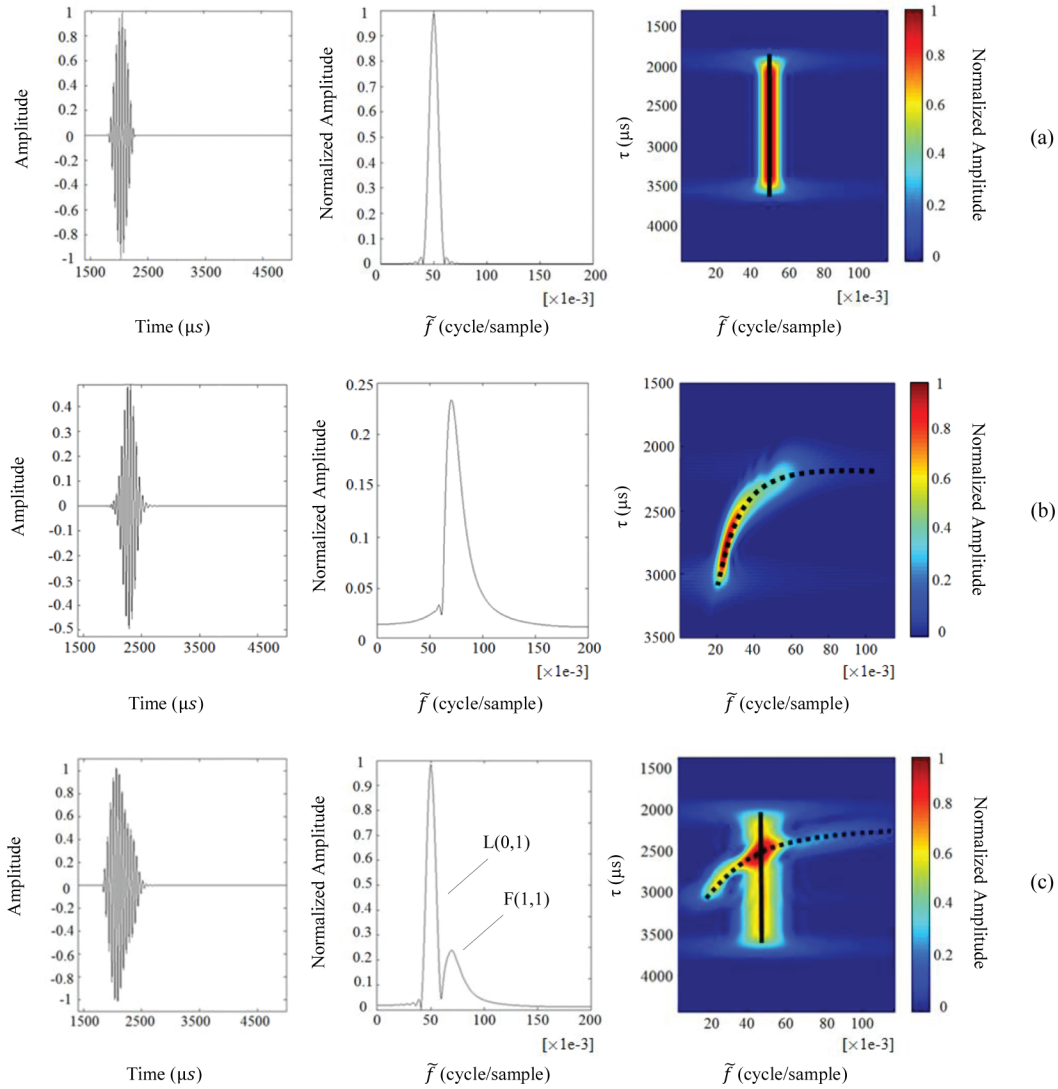


Fig. 3. From left to right: signal, frequency sweep spectrum (FSS), and total frequency sweep spectrum (TFSS) of (a) nondispersive L(0,1) and (b) dispersive F(1,1); (c) Superposition of (a) and (b).

vidual samples at the corresponding rate-converted frequency-sweep acquisitions.

After the application of Fourier transform on ASWs, FSSs are obtained, as shown in Fig. 3(middle). The distinct peaks illustrated in Fig. 3(middle) correspond to the identified wave modes of interest in the superposed wave packet shown in Fig. 3(c)(left).

TFSS shown in Fig. 3(right) represents all of the FSSs meshed together at each of their respective rate-converted time instants. The nondispersive L(0,1) wave mode exhibits a constantly increasing shift in rate-converted time, (Section II-D, Fig. 2) so the position of the peak which is observed in the FSS( $\tilde{f}$ ) and TFSS( $\tilde{f}, \tau$ ) [Fig. 3(a)(middle) and (right)] remains constant. However, the dispersive F(1,1) wave mode exhibits a nonlinearly increasing shift in rate-converted time causing a variation in the position of the peak observed in the FSS( $\tilde{f}$ ) and TFSS( $\tilde{f}, \tau$ ) [Fig. 3(b)(middle) and (right)]. As was discussed in Section II-C, the ToF of each wave mode at  $f_0$  frequency, i.e., 20 kHz, is extracted by capturing the presence of a new gradually

rising magnitude spectrum at each successive time instant. Given the ToF, the group velocity was estimated according to (16). Fig. 5 represents the computed F(1,1) and L(0,1) dispersion curve mapped to the dispersion curve given by Disperse.

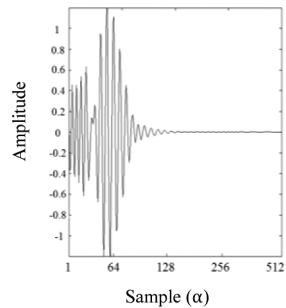


Fig. 4. Amplitude sweep wave form (ASW) at 2300 μs.

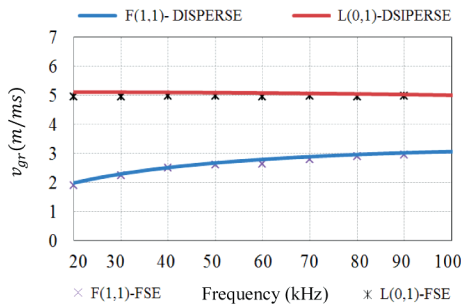


Fig. 5. Group velocity dispersion curve of the aluminum rod.

IV. EXPERIMENTAL VALIDATION

The technique is applied to pulse-echo UGW signals from an aluminum rod. The data are acquired according to Section IV-B and analyzed using the FSE technique in Section IV-C. The group velocity dispersion curve of the specimen is also extracted from the given results and validated via Disperse.

A. Experimental Setup

The experimental set-up is illustrated in Fig. 6. A shear piezoelectric transducer [25] is orientated in a manner that allows it to actuate longitudinally in the axial direction of the 2.15-m-long aluminum rod with 8 mm diameter. The transducer was connected to the unit via a tool lead cable and then the unit was connected to the laptop by communication cable. A ten-cycle Hann windowed signal was injected from the laptop to the unit and fired from the transducer through the rod.

B. Data Collection and Experimental Results

In this experiment, several UGW signals were collected from the rod with different frequencies and an equal incremental factor. With reference to Section II-A, 512 frequency-sweep excitations are performed in a wide range of frequencies starting from 20 kHz ( $f_0$ ) and stopping at 100 kHz ( $f_{p-1}$ ).

Fig. 7(left) displays the acquisition collected at  $f_0$ . It displays multimodal reflection from the end of the rod

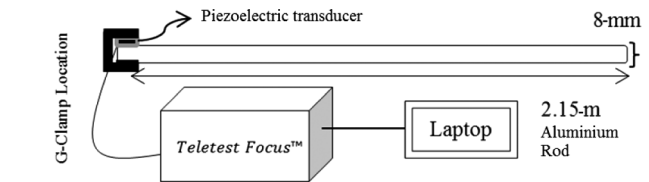


Fig. 6. Experimental setup.

with overlapped echoes at different ToFs. It is notable that the first echo of L(0,1) was ignored therefore the acquisition could be analyzed with a challenging scenario where several echoes are strongly overlapped.

The total signal acquisitions are accumulated as an input to the sampling rate conversion. Figs. 7(middle) and (right) and Fig. 8 represent sample ASW( $\alpha$ ) and FSS( $\tilde{f}$ ) at chosen individual rate-converted time instants, respectively. The  $x$ -axis in Figs. 7(middle) and (right) represents the individual samples collected at the corresponding rate-converted frequency-sweep acquisitions. Fig. 9 displays the TFSS( $\tilde{f}, \tau$ ) derived from the superposed signals.

C. Group Velocity Extraction and Further Analysis

According to (16) the group velocities of the modes of interest were estimated and compared with the values given by Disperse in Fig. 10. Although T(0,1) could be theoretically generated within the frequency range that has been excited, the orientation of the piezoelectric transducer is aligned to the axial direction of the rod, hence this restricts any displacements in the circumferential direction. Therefore, the presence of T(0,1) in this set of experiments will be negligible. It is also notable that according to the dispersion curve of the specimen, the cut-off frequency of L(0,2) is approximately at 460 kHz, which is beyond the frequency range of excitation.

Here, the mode conversion occurred [9], [26]–[29] because the transducer is clamped on the end of the rod via a G-clamp. The rod surface is in contact with the piezoelectric ceramic at an arbitrary point on the circumference and the reactive force of the clamp surface is in contact with the rod directly 180° to the prior mentioned arbitrary point. The location at which the transducer and clamp are situated produces a feature on the rod; hence, after the

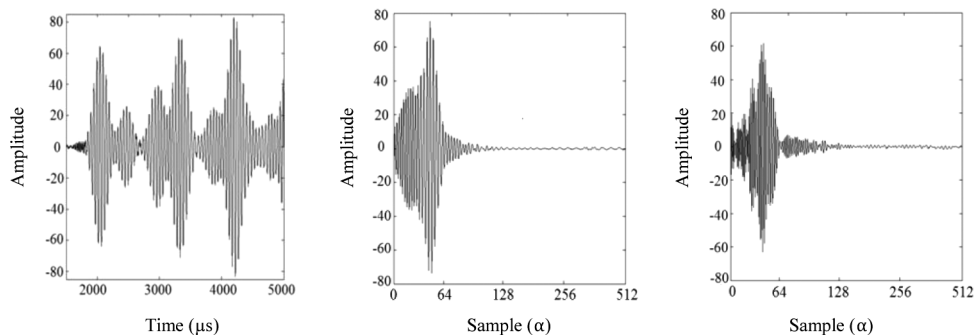


Fig. 7. (left) Acquisition at  $f_0$ , (middle) amplitude sweep wave form (ASW) at 2300  $\mu$ s, (right) ASW at 4300  $\mu$ s.

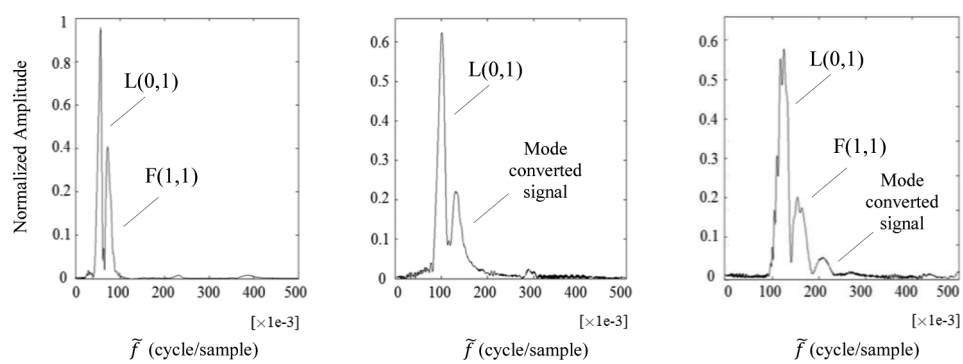


Fig. 8. Frequency sweep spectrum (FSS) at (left) 2300  $\mu\text{s}$ , (middle) 3500  $\mu\text{s}$ , (right) 4300  $\mu\text{s}$ .

reflection of the waves from the end of the rod toward the clamp and the transducer, the longitudinal wave converts to a flexural wave and/or a generated flexural wave has been converted into a longitudinal mode. This produces an additional wave packet in the acquisition with relatively lower amplitude than the other echoes. This mode-converted wave packet possesses the same velocity as L(0,1) because it has the same round trip time [26].

Having the capability to identify and discriminate the wave modes with their velocity makes the defect detection process straightforward, where the end of the rod can be treated as a defect of interest which produces mode conversions.

The distinct curves illustrated in Fig. 9 are traced energy peaks which show the existing superposed wave modes with different gradients at successive echoes. As discussed in Section II-D, during the technique implementation, the original time range has been shortened to highlight the presence of the longitudinal, flexural, and converted wave modes at different rate-converted times. The wave modes were identified according to their group velocity value given in Fig. 10. Fig. 9(left) represents the superposition of the second echo of L(0,1) and first echo of F(1,1) in the given time range of 1400 to 6400  $\mu\text{s}$ . The L(0,1) wave mode shows a constantly increasing shift in rate-converted time (Section II-D, Fig. 2), so the position of the L(0,1) peaks which are observed in the FSS( $\tilde{f}$ ) and

TFSS( $\tilde{f}, \tau$ ) (Figs. 8 and 9) remain constant. However, the dispersive F(1,1) wave mode exhibits a nonlinearly increasing shift in rate-converted time, causing the nonlinear variation in the position of the F(1,1) peaks observed in the FSS( $\tilde{f}$ ) and TFSS( $\tilde{f}, \tau$ ) (Figs. 8 and 9). Fig. 9(middle) represents the superposition of third echo of L(0,1) and first echo of the mode-converted signal over the given rate-converted time 2000 to 8500  $\mu\text{s}$ . Fig. 9(right) represents the superposition of three wave modes arising because of the reflection and mode conversion at the clamped end of the rod at a given time range of 3500 to 10000  $\mu\text{s}$ . The FSE procedure was performed in sequence with a given gradual change in  $f_0$  frequency, therefore a portion of the group velocity dispersion curve covering the frequency range of excitation was measured and validated via Disperse in Fig. 10.

According to the given results, the proposed technique shows promise for wave mode identification in a multimodal UGW signal. It is also demonstrated to have the capability to plot the group velocity dispersion curve of an aluminum rod. Therefore, the technique is mostly expected to be suitable for reliable inspection of one-dimensional structures (e.g., wires, bars, pipes, rails, etc.) in field inspections, because it requires a frequency-sweep pulse-echo measurement.

It is notable that the time-domain separation has not been performed in this paper because the objective of the

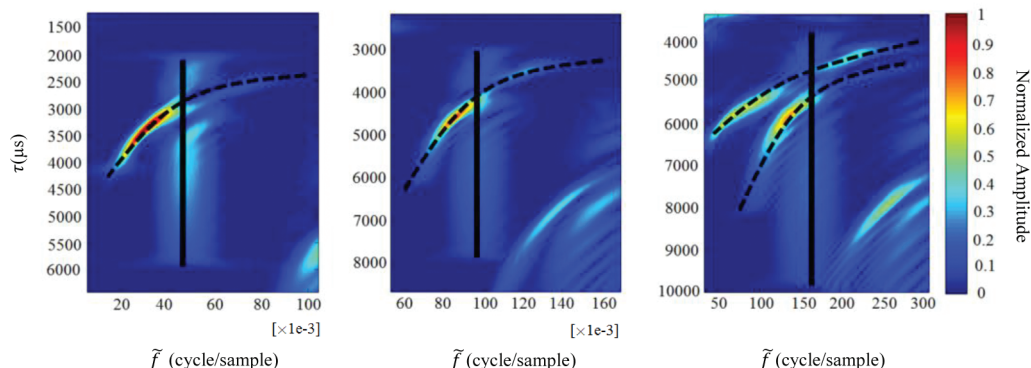


Fig. 9. Total frequency sweep spectrum (TFSS) image of (left) second echo L(0,1) and first echo F(1,1); (middle) third echo L(0,1) and first echo mode-converted signal; (right) fourth echo L(0,1), second echo F(1,1) and second echo mode-converted signal.



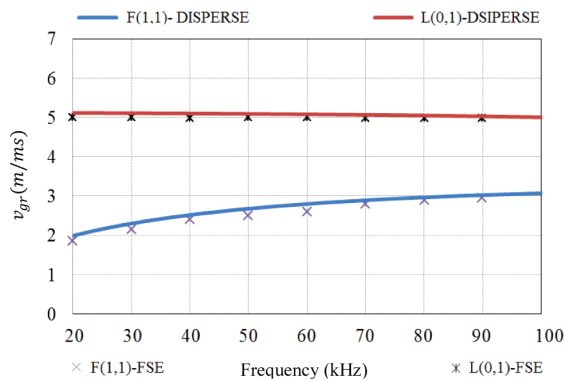


Fig. 10. Validation of experimental group velocity dispersion curve. 

paper was wave mode identification focused in the Fourier domain. According to the potentials of the proposed technique that have been highlighted throughout the paper, the authors suggest employing customized filters on FSS responses to extract individual time-domain wave forms; therefore, it could also be particularly beneficial in practical applications, e.g., defect sizing and attenuation measurements out in the field.

## V. CONCLUSIONS

In this paper, a frequency-sweep examination (FSE) technique was introduced and showed promise for defect detection in complex UGW inspections. It has been empirically demonstrated that the proposed signal processing technique is useful for ToF/group velocity extraction and wave mode identification of superposed UGWs. The technique obtained the number of present wave modes with accurate quantitative information allowing a portion of group velocity dispersion curve to be computed.

The assumption of a known propagation distance is a drawback of the technique which must be taken into account in field inspection, as well as the one presented by TFR methods [13] and [15]. In addition, the time-domain separation has not been performed in this paper because the paper is mainly focused on wave mode identification, which was achieved in the Fourier domain. According to the potentials of the proposed technique, customized filtering in the FSS domain can be a possible solution to such a requirement.

The advantage of this approach over spatial 2-D-FFT [5] or SVD [12] measurements is that it is based on performing pulse-echo frequency-sweep excitations of UGWs rather than several pitch-catch measurements. Moreover, the use of FSE enables the empirical computation of the dispersion curve, which overcomes the need for *a priori* knowledge, whereas it is needed for dispersion compensation methods [15].

The future work on this topic will focus on empirically plotting the entire phase and group velocity dispersion curves assuming that the length of the structure is unknown.

## ACKNOWLEDGMENTS

The primary acknowledgement of the authors is to the *IEEE Transactions on Ultrasonics, Ferroelectrics, and Frequency Control* reviewers for their constructive comments that helped to improve the manuscript. The authors also gratefully acknowledge their colleagues at TWI and Plant Integrity Ltd., especially Dr. P. Jackson, Dr. P. Mudge, Dr. A. Haig, Dr. B. Engineer and Mr. K. Thornicroft for their inputs and useful discussions.

## REFERENCES

- [1] P. Catton, "Catton, P, 2008, Long range ultrasonic guided waves for the quantitative inspection of pipelines," Eng.D. thesis, School of Engineering and Design, Brunel University, London, England, 2009, pp. 2–4.
- [2] J. L. Rose, "Successes and challenges in ultrasonic guided waves for NDT and SHM" in *Proc. National Seminar & Exhibition on Non-Destructive Evaluation*, 2009, pp. 2–10.
- [3] J. Krautkramer and H. Krautkramer, *Ultrasonic Testing of Materials*, 4th ed., New York, NY: Springer Verlag, 1990.
- [4] B. Pavlakovic, M. J. S. Lowe, D. N. Alleyne, and P. Cawley, "Disperse: A general purpose program for creating dispersion curves," in *Rev. Progress Quantitative Nondestructive Evaluation*, 1997, vol. 16, pp. 185–192.
- [5] D. Alleyne and P. Cawley, "A two-dimensional fourier transform method for the measurement of propagating multimode signal," *J. Acoust. Soc. Am.*, vol. 89, no. 3, pp. 1159–1168, 1991.
- [6] W. H. Prosser and M. D. Seale, "Time-frequency analysis of the dispersion of Lamb modes," *J. Acoust. Soc. Am.*, vol. 105, no. 5, pp. 2669–2676, 1999.
- [7] P. Wilcox, M. Lowe, and P. Cawley, "The effect of dispersion on long-range inspection using ultrasonic guided waves," *NDT Int.*, vol. 34, no. 1, pp. 1–9, 2001.
- [8] R. Sicard, J. Goyette, and D. Zellouf, "A numerical dispersion compensation technique for time recompression of Lamb wave signals," *Ultrasonics*, vol. 40, no. 1–8, pp. 727–732, 2002.
- [9] P. Wilcox, "A rapid signal processing technique to remove the effect of dispersion from guided wave signals," *IEEE Trans. Ultrason. Ferroelectr. Freq. Control*, vol. 50, no. 4, pp. 419–427, 2003.
- [10] K. Toiyama and T. Hayashi, "Pulse compression technique considering velocity dispersion of guided wave," in *34th Annu. Rev. Prog. Quantitative Nondestructive Evaluation*, 2008, vol. 975, pp. 587–593.
- [11] H. Kuttig, M. Niethammer, S. Hurlbauss, and L. J. Jacobs, "Model based analysis of dispersion curves using chirplets," *J. Acoust. Soc. Am.*, vol. 119, no. 4, pp. 2122–2130, 2006.
- [12] J. G. Minonzio, M. Talmant, and P. Laugier, "Measurement of guided mode phase velocities using multi-emitters and multi-receivers arrays in contact and transmission matrix analysis: Application to cortical bone evaluation," in *IEEE Int. Ultrasonics Symp. Proc.*, 2009, pp. 1–4.
- [13] K. Xu, D. Ta, and W. Wang, "Multiridge-based analysis for separating individual modes from multimodal guided wave signals in long bones," *IEEE Trans. Ultrason. Ferroelectr. Freq. Control*, vol. 57, no. 11, pp. 2480–2490, 2010.
- [14] X. Song, D. Ta, and W. Wang, "Analysis of superimposed ultrasonic guided waves in long bones by the joint approximate diagonalization of eigen-matrices algorithm," *Ultrasound Med. Biol.*, vol. 37, no. 10, pp. 1704–1713, 2011.
- [15] K. Xu, D. Ta, P. Moilanen, and W. Wang, "Mode separation of Lamb waves based on dispersion compensation method," *J. Acoust. Soc. Am.*, vol. 131, no. 4, pp. 2714–2722, 2012.
- [16] A. H. Nuttall, "Some windows with very good sidelobe behaviour," *IEEE Trans. Acoust. Speech Signal Process.*, vol. 291, no. 1, pp. 84–91, 1998.
- [17] P. Cawley and D. N. Alleyne, "The use of Lamb waves for the long-range inspection of large structures," *Ultrasonics*, vol. 34, no. 2, pp. 287–290, 1996.
- [18] T. J. Terrell and L.-K. Shark, *Digital Signal Processing*. London, UK: Macmillan Press, 1996, ch. 1, pp. 10–12.

- [19] J. Watkinson, *The Art of Digital Audio*, 1st ed., London, UK: Focal Press, 1988, pp. 122–135.
- [20] The MathWorks Inc. (2013, Jun.) Matlab mathematics: User's guide (R2013a), pp. 7–20 to 7–35. [Online]. Available: [http://www.mathworks.co.uk/help/pdf\\_doc/matlab/math.pdf](http://www.mathworks.co.uk/help/pdf_doc/matlab/math.pdf)
- [21] R. E. Crochiere and L. R. Rabiner, "Interpolation and decimation of digital signals—A tutorial review," *Proc. IEEE*, vol. 69, no. 3, pp. 300–330, 1981.
- [22] P. Cawley and D. Alleyne, (2013, Sep.) "Paraactical long range guided wave inspection—Managing complexity," Feb. 2004. [Online]. Available: <http://www.ndt.net/article/mendt03/4/4.htm>
- [23] A. V. Oppenheim and R. W. Schaffer, *Digital Signal Processing*, ed. 1, London, UK: Prentice Hall Int., 1975, pp. 239–242.
- [24] A. H. Meitzler, "Mode coupling occurring in the propagation of elastic pulses in wires," *J. Acoust. Soc. Am.*, vol. 33, no. 4, pp. 435–445, 1961.
- [25] Plant Integrity Ltd., "Teletest focus long range ultrasonic system specification," TWI- The Welding Institute, Cambridge, United Kingdom, Feb. 6, 2007.
- [26] E. P. Papadakis, "Effect of multimode guided-wave propagation on ultrasonic phase velocity measurements: problem and remedy," *J. Acoust. Soc. Am.*, vol. 45, no. 6, pp. 1547–1555, 1969.
- [27] M. J. S. Lowe, D. N. Alleyne, and P. Cawley, "The mode conversion of a guided wave by a part circumferential notch in a pipe," *J. Appl. Mech.*, vol. 65, no. 3, pp. 649–656, 1999.
- [28] A. Demma, P. Cawley, M. Lowe, and A. G. Roosenbrand, "The reflection of the fundamental torsional mode from cracks and notches in pipes," *J. Acoust. Soc. Am.*, vol. 114, no. 2, pp. 611–625, 2003.
- [29] A. Demma, P. Cawley, M. Lowe, A. G. Roosenbrand, and B. Pavlakovic, "The reflection of guided waves from notches in pipes: A guide for interpreting corrosion measurements," *NDT&E Int.*, vol. 37, no. 3, pp. 167–180, 2004.



**Sina Fateri** received his B.Sc. (Honours) degree in computer science from the University of Mazandaran, Babolsar, Iran, in 2009 and his M.Sc. (Distinction) degree in wireless communications engineering from Brunel University, London, England, in 2011. He was a graduate teaching assistant for the Wireless Communications laboratory from 2011 to 2013. He is currently pursuing the Ph.D. degree in electronic systems research (CESR) at Brunel University, based in TWI Ltd., Cambridge, England. His research is focused on

advanced signal processing techniques for ultrasonic guided wave inspections. His research interests are acoustic signal processing, mode identifications in ultrasonic guided wave inspections, and ultrasonic guided-wave mode conversion from discontinuities.



**Nikolaos V. Boulgouris** (S'96–M'04–SM'09) is a Senior Lecturer with the Department of Electronic and Computer Engineering at Brunel University, UK. From December 2004 to August 2010, he served as a Lecturer and a Senior Lecturer at King's College London, London, UK. From 2003 to 2004, he was a Post-Doctoral Fellow with the Department of Electrical and Computer Engineering of the University of Toronto, Canada. He received the Ph.D. degree from the Electrical and Computer Engineering Department of the University of Thessaloniki, Greece, in 2002. Dr. Boulgouris served as a guest co-editor for two journal special issues and was co-editor of the book *Biometrics: Theory, Methods, and Applications*, published by Wiley–IEEE Press in 2009. Dr. Boulgouris served as an Associate Editor for the *IEEE Transactions on Image Processing* from 2010 to 2014 and for the *IEEE Signal Processing Letters* from 2007 to 2011.



**Adam Wilkinson** was born in Birmingham, UK, in 1969. He read engineering at Sidney Sussex College, Cambridge, and obtained a Ph.D. degree in magnetic resonance imaging from University of Cambridge. He is currently a Principal Project Leader at Plant Integrity Ltd. with interests in guided ultrasound, structural health monitoring, embedded electronics and software, cross-platform rapid application development tools and communications systems.



**Wamadeva Balachandran** is a Research Professor and Director of Centre for Electronic Systems Research (CESR) at Brunel University, UK. He is a Fellow of IEEE (USA), the Institution of Engineering and Technology (UK), the Institute of Physics (UK), the Institute of Measurement and Control (UK), and the Royal Society of Arts (UK). He served as Head of the Department of Systems Engineering at Brunel University from 1999 to 2004. He was a Visiting Professor in the Driftmier Engineering Centre at the University of

Georgia in 1993 and 1996. He has been a Visiting Professor at the University of Mansoura, Egypt, and Dongguan University, China, since 1993 and 1996, respectively. In 2004, he was a Visiting Scholar in the School of Engineering and Applied Science at the University of California, Los Angeles. His research interest spans several different disciplines: electrostatics and charged particle dynamics, electrohydrodynamics, micro/nano technologies, microengineered devices for POCT, biosensors, fingerprint biometrics, global positioning satellite system for blind navigation, ultrasonic and EMAT NDT, electron beam and microwave plasma for environmental pollution control, and medical electronics. He has actively pursued research in these interdisciplinary fields for more than 30 years, publishing more than 350 papers to date and filing 15 patent applications. He has presented more than 45 plenary and invited talks in his field of expertise at international conferences around the globe. He was a recipient of the IEEE John Melcher best paper award and innovation and creativity awards in 2000 and 2004, respectively. He continues to review manuscripts for 15 archival journals and research grant applications for EPSRC (UK), EU Framework, NSF (USA), NSERC (Canada), the Greek government, Lockheed Martin, the Swiss Research Council, the Portuguese Research Council, and the Singapore government.



**Tat-Hean Gan** graduated with first-class honours degree in electrical and electronics engineering from the University of Nottingham. He went on to pursue his M.Sc. degree in advanced mechanical engineering and graduated with a Distinction from the University of Warwick in 1998, and continued his Ph.D. studies in engineering specializing in advanced ultrasonic imaging at the same University. In 2006, he completed his Executive MBA degree at the University of Birmingham. He has worked as an academic and in industry for many years. He has published more than 100 papers and has contributed to several books in the field of nondestructive testing (NDT). Tat-Hean is currently a Professor at Brunel University, where he is also the Chair of Acoustic Waves Technologies in the School of Engineering and Design. His research interest is in signal and image processing, sensor development, asset integrity management, and structural assessment. He has obtained his CEng, EurIng and IntPE(UK) status and he has been a Fellow of the Institute of Engineering and Technology (IET) and British Institute of Non-Destructive Testing since 2011. Tat-Hean is also an Associate Director at TWI Ltd., and Technology Director of the National Structural Integrity Research Centre (NSIRC), the UK's first industry-led postgraduate education and research center in structural integrity.